Polymer Journal (2019) 51:161–171
https://doi.org/10.1038/s41428-018-0135-6

ORIGINAL ARTICLE

Microscopic structural response of nanoparticles in styrene–butadiene rubber under cyclic uniaxial elongation

Yuya Shinohara[1,3] · Hiroyuki Kishimoto[2] · Tomomi Masui[2] · Shota Hattori[1] · Naoko Yamaguchi[1] · Yoshiyuki Amemiya[1]

Received: 18 August 2018 / Revised: 18 September 2018 / Accepted: 19 September 2018 / Published online: 30 October 2018
© The Society of Polymer Science, Japan 2018

Abstract

Changes in the aggregated structure of silica in styrene–butadiene rubber are measured with small-angle X-ray scattering under cyclic uniaxial elongation. We employ a spherical harmonics expansion approach to quantitatively analyze the anisotropic scattering data and to separate the anisotropic response of the silica's configuration upon the elongation from the isotropic component. The results clearly show inhomogeneity in microscopic deformation upon elongation. Phase lag between microscopic structural responses and macroscopic strain are also observed. This study demonstrates that the combination of time-resolved small-angle scattering measurement and an analysis using spherical harmonics expansion is quite useful for exploring the structural response of filled rubber systems to an external deformation.

Introduction

Addition of nanoparticles such as carbon black and silica to rubber leads to changes in their mechanical and viscoelastic properties. This reinforcement effect plays a critical role in controlling the viscoelastic properties of industrial products such as vehicle tires, and many studies have been conducted to elucidate its physical picture. Nanoparticles usually show hierarchical structures: primary particles form an aggregate, and the aggregates form an agglomerate, etc [1]. The presence of this hierarchy makes the quantitative structural analysis of filled rubber challenging [1–6]. The aggregate structure of filler and its change upon deformation have been studied using various techniques, such as ultra-small-angle X-ray scattering (USAXS) and ultra-small-angle neutron scattering (USANS) [1–8]. These methods have been utilized for measuring the static structure of filler aggregates and its changes upon large deformation. Although changes in hierarchical structures of filler under a large strain are vital to discuss the mechanical properties of nanocomposites, they are not useful for explaining the viscoelastic properties such as frequency dependence of viscoelastic modulus. For example, one of the critical parameters that characterize the products' energy loss is loss tangent, $\tan\delta$. This quantity is defined as the phase delay between stress and strain and can be measured by cyclic shear measurement via the relationship $\tan\delta = G''/G'$, where G' and G'' are an elastic modulus and a loss modulus, respectively. Loss tangent is used to discuss the viscoelastic properties, particularly those for energy loss, and is defined macroscopically; its microscopic picture is, however, not clarified by the static structure nor the structural change under large deformation.

Structural analysis of filled rubber under cyclic strain will give an answer to the above question. In the case of rubber filled with nanoparticles, the X-ray scattering intensity at a small scattering angle mainly originates from the distribution of nanoparticles due to the high electron-density contrast between nanoparticles and rubber. Thus, measurement of the scattering of filled rubber under cyclic strain directly

✉ Yuya Shinohara
yshinoha@utk.edu

[1] Department of Advanced Materials Science, Graduate School of Frontier Sciences, The University of Tokyo, 5-1-5 Kashiwanoha, Kashiwa, Chiba 277-8561, Japan

[2] Sumitomo Rubber Industries Ltd., 2-1-1, Tsutsui, Chuo, Kobe, Hyogo 651-0071, Japan

[3] Present address: Shull-Wollan Center, University of Tennessee, Knoxville and Oak Ridge National Laboratory, Oak Ridge, TN, USA

provides structural information of the nanoparticle configuration in stretched rubber. It is, however, not easy to extract the structural information from such an experiment. First, the presence of hierarchy and polydispersity in nanoparticle size and shape complicate the interpretation of scattering intensity profiles as noted above. Second, the cyclic measurement usually needs to be done with a minimal strain to escape from the complexity of nonlinear response upon a more significant strain. This small strain makes structural analysis difficult because the expected structural changes are small compared to those in large-strain experiments. Thanks to recent developments in X-ray detectors and a long sample-to-detector distance with a highly directional X-ray from a synchrotron X-ray source, tiny changes in scattering intensity profiles can be measured as shown in this study.

Another difficulty lies in the analysis scheme of scattering profiles from deformed rubber samples. Despite significant effort by many researchers, structural information, particularly under deformation, remains elusive or lacks quantitative information. One of the reasons, for example in the case of uniaxial elongation, is that scattering intensity profiles are analyzed only in a direction parallel to the elongation and its perpendicular direction. A butterfly-like anisotropy is commonly observed [9–14], but its analysis remains a qualitative comparison of scattering images and/or a one-dimensional slice of scattering profiles in either reciprocal or real space [7, 15, 16]. These simplified analyses may have been justified when only one-dimensional measurement using a Bonse-Hart camera was available for USAXS/USANS. However, a high-quality two-dimensional scattering image at ultra small scattering angle is available now thanks to advances in X-ray sources, optics, and detectors [17]. Therefore, two-dimensional scattering patterns, or rather three-dimensional scattering patterns in a reciprocal space, need to be directly studied for discussing any kind of anisotropic scattering data. For that, more elaborate techniques are required to quantitatively describe the anisotropic scattering patterns.

Recently, the use of spherical harmonics was successfully introduced to the SANS analysis of deformed samples [18, 19]. For shear and uniaxial elongation, symmetric structural changes are reasonably assumed, and the anisotropic characteristics can be quantitatively extracted. The analysis of anisotropic scattering pattern using spherical harmonics has been used for metallic glass and polymer either via anisotropic structure factors or an anisotropic pair distribution function [18–23]. In the current study, we introduce this method for analyzing the anisotropic pattern from the stretched rubber samples.

The overarching goal of this study is to find connections between macroscopic properties and microscopic structure and dynamics of filled rubber, thereby obtaining a physical picture of the reinforcement effect for improving its viscoelastic properties. In this paper, we focus on the observation of the anisotropic response of silica aggregates to cyclic uniaxial elongation with time-resolved small-angle X-ray scattering (SAXS) measurements combined with dynamic viscoelastic measurements. The samples were sinusoidally stretched, and the scattering at each phase was measured. We introduced analyses using spherical harmonic expansion [18] instead of conventional methods that analyze the scattering intensity profiles only along elongation direction and its vertical direction. We also conducted heterodyne X-ray Photon Correlation Spectroscopy (XPCS) measurements [24, 25] to obtain further information about the response of filler aggregate structure upon strain.

Materials and methods

Materials

Commercially available solution styrene–butadiene rubber (Buna® VSL 4720, Lanxess Corp.) filled with commercially used silica particles (Ultrasil VN3, Evnik Industries AG) was used as the sample. The details of the materials and the sample codes are shown in Table 1. The average size of the primary silica particles was 13 nm from TEM observation. Two different types of silane-coupling agent were used: polysulfide bis(triethoxysilylpropyl)polysulfide (Si266®) and NXT (mercapto-functional silane). We also prepared the sample without silane-coupling agent. Rubber was cross-linked using sulfur with accelerator (Acc. NS and DPG). Rubber was cross-linked at 170 °C for 12 min.

SAXS under cyclic strain

Combined measurement of SAXS and dynamical viscoelasticity was conducted at BL08B2, SPring-8 (Hyogo, Japan). The X-ray energy was 8 keV, and the distance between samples and a detector was 15.7 m, which was calibrated using the diffraction from a grating of a 100 nm grating period. A pixel-array detector (PILATUS 100 K, Dectris ltd.) [26] was used to measure SAXS images. Rectangular-shaped samples (4 mm in width and ~0.5 mm in thickness) were set at a viscoelastic spectrometer (RheoGel E-4000, UBM ltd., Japan). Prior to the measurement, the samples were stretched to $\frac{\Delta L}{L_0} = 0.3$, where ΔL and L_0 are the amounts of stretching and the length of the undeformed sample, to remove mechanical history. Then, they were prestretched to $\frac{\Delta L}{L_0} = 0.2$ and were afterward sinusoidally stretched with a stretching ratio of $\frac{\Delta L}{L_0} = 0.02$ during the X-ray scattering measurement. The length of the sample is thus expressed as follows:

$$L(t) = L_0(1.2 - 0.02\ \sin(2\pi ft)). \quad (1)$$

Table 1 Sample details. Weight fraction is shown

Sample code	S1	S2	S3	N1	N2	N3	W1	W2	W3
SBR (VSL4720)	100	100	100	100	100	100	100	100	100
Silica	24.5	55	94.5	24.5	55	94.5	24.5	55	94.5
Si266	1.96	4.4	7.56						
NXT				1.96	4.4	7.56			
Sulfur	1.5	1.5	1.5	1.5	1.5	1.5	1.5	1.5	1.5
Acc. NS	1	1	1	1	1	1	1	1	1
Acc. DPG	1	1	1	1	1	1	1	1	1
d_c/nm	$(1.4 \pm 0.4) \times 10^2$	$(7.6 \pm 2.7) \times 10$	$(4.7 \pm 1.4) \times 10$	$(1.5 \pm 0.6) \times 10^2$	$(8.7 \pm 2.5) \times 10$	$(5.2 \pm 2.4) \times 10$	$(1.5 \pm 0.8) \times 10^2$	$(1.0 \pm 0.2) \times 10^2$	$(4.8 \pm 1.7) \times 10$

Uncertainties in d_c are estimated by using the width of the peak in the Kratky plot

Acc accelerator, *DPG* 1,3-diphenylguanidine, d_c averaged distance between aggregates estimated for undeformed samples by SAXS

The frequency of stretching, f, was 0.1, 1, and 10 Hz. The trigger signal was sent from the viscoelastic spectrometer to produce a delayed trigger pulse signal. This delayed trigger was used to drive the X-ray detector. The cycle is divided into ten parts, and SAXS images were recorded at each part as shown in Fig. 1a. The temperature of the samples was set at 0, 25, and 50 °C. The transmittance of samples was measured by a set of ion chambers that were placed up- and downstream of a sample.

XPCS of stretched samples

XPCS measurement of stretched rubber was conducted at BL03XU, SPring-8 (Hyogo, Japan) [27]. A set of pinholes (20 and 50 µm in diameter) was used to produce quasi-coherent X-rays and to remove parasitic scattering. The samples were set at a uniaxially stretching instrument (RheoGel S-1000, UBM ltd., Japan). Moreover, a plate of glassy carbon was placed in front of the sample, and the interference between the scattering from the samples and that from the static glassy carbon was observed [25]. Stretched sample was illuminated with 8 keV X-rays. The size of the X-ray beam at the sample position was 25 µm. The speckle pattern was measured with a CCD detector (C4880-50, Hamamatsu Photonics Ltd., Japan) coupled with an X-ray image intensifier (Hamamatsu Photonics Ltd., Japan) [28]. Before the measurement, samples were stretched to $\frac{\Delta L}{L_0} = 0.3$ to remove mechanical history. Then, they were stretched to $\frac{\Delta L}{L_0} = 0.2$, and the distance between the chucks was kept constant. XPCS measurements were started just after the distance reached the preset values. The exposure time was 50 ms, and the image was recorded each 2 s. The stress was recorded during the XPCS measurement.

Analysis of time-resolved SAXS

Measured 2D-SAXS spectra were analyzed using a spherical harmonic expansion approach [18]. Here, we briefly introduce the outline: see the reference for details [18]. On the assumption that there is no multiple scattering, no polydispersity in particle size or shape and that particles are spherical, the scattering intensity, $I(\boldsymbol{Q})$, can be factorized in the context of small-angle X-ray scattering as

$$I(\boldsymbol{Q}) = BS(\boldsymbol{Q})F(\boldsymbol{Q}) \tag{2}$$

where $\boldsymbol{Q}$ is the momentum transfer and B is a coefficient. $S(\boldsymbol{Q})$ and $F(\boldsymbol{Q})$ represent interparticle structure factor and particle structure factor, respectively. As discussed in a previous study [18], the structure factor of silica particles, $S(\boldsymbol{Q})$, can be expressed in terms of spherical harmonics:

$$S(\boldsymbol{Q}) = \sum_{l,m} S_l^m(Q) Y_l^m(\theta, \varphi) \tag{3}$$

where Q and $Y_l^m(\theta, \varphi)$ are the magnitude of $\boldsymbol{Q}$ and the real spherical harmonic functions of degree l and order m, respectively. θ is the polar angle from the positive Q_z axis with $\theta \in [0, \pi]$, and φ is the azimuthal angle in the Q_x-Q_y plane from the Q_x axis with $\varphi \in [0, 2\pi)$. In this study, the stretching is along the Q_z axis, and the incident X-ray beam is perpendicular to the Q_x−Q_z plane (Fig. 1c). As discussed in detail in previous studies [18, 19], the expression is greatly simplified in the case of uniaxial extension, and all $m \neq 0$ terms and odd l terms can be ignored. The three leading anisotropic spherical harmonics, $Y_2^0(\theta)$, $Y_4^0(\theta)$, and $Y_6^0(\theta)$, are shown in Fig. 1b. The cross-section of $S(\boldsymbol{Q})$ on the Q_xQ_z plane is given by

$$S(Q_x, Q_y = 0, Q_z) = \sum_{l:\text{even}} S_l^0(Q) Y_l^0(\theta). \tag{4}$$

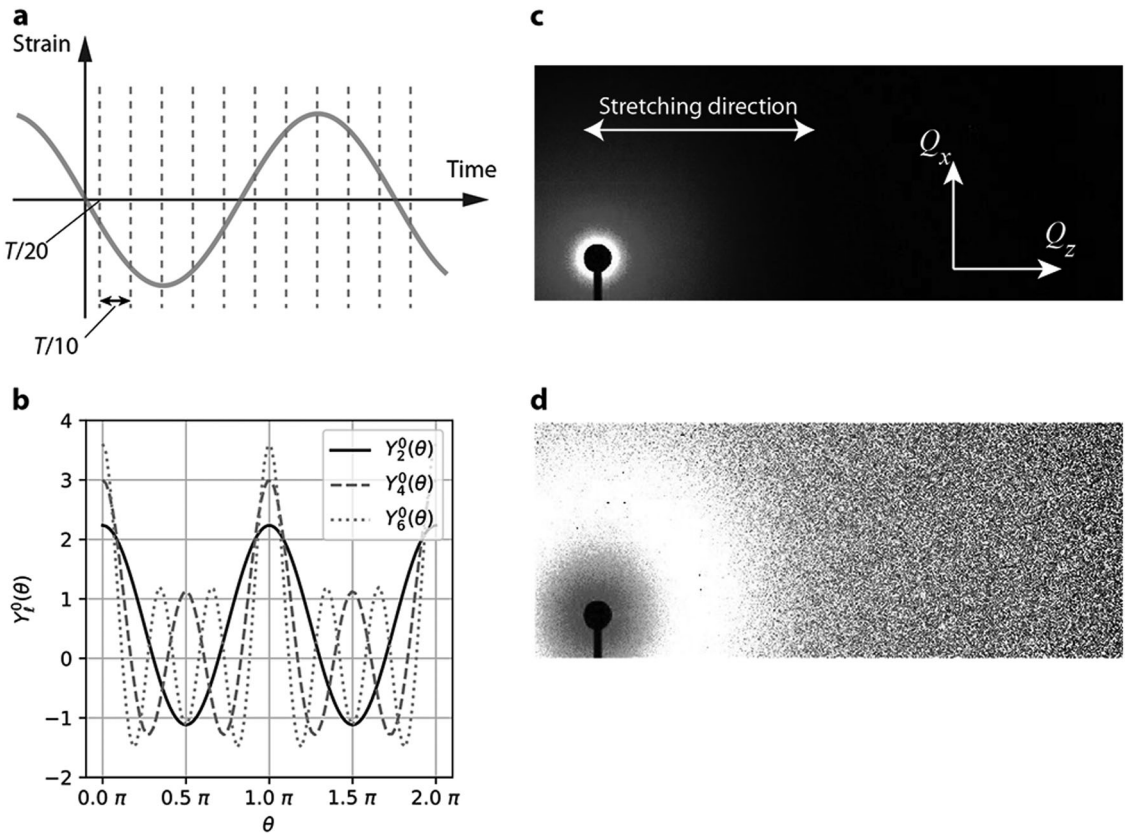

Fig. 1 **a** Sample was sinusoidally stretched. A single period was divided into ten frames, and the scattering image was recorded at each frame. The first frame starts at *T*/20, and the exposure time for each frame was *T*/10. **b** Profiles of real spherical harmonic functions $Y_2^0(\theta)$, $Y_4^0(\theta)$, and $Y_6^0(\theta)$. **c** An example of a two-dimensional scattering image of stretched rubber. Sample was stretched in the *z*-direction, and X-ray impinged on the sample along a direction perpendicular to the *x*–*z* plane (*y*-direction). **d** Kratky representation ($Q^2I(Q)$) of the same stretched sample. Distorted ring pattern originating from the inter-aggregate correlation becomes visible

Here, Q_Z is parallel to the stretching direction, and Q_y is parallel to the incoming X-rays. Because $Y_l^0(\theta)$ forms an orthogonal basis set not only in 3D space but also on the *xz* plane [18], the expansion coefficient $S_l^0(Q)$ can be computed as

$$S_l^0(Q) = \tfrac{1}{2}\int_0^\pi S(Q,\theta)Y_l^0(\theta)\sin\theta d\theta. \quad (5)$$

In this study, we calculate the expansion coefficient of scattering intensity, $I(Q)$, instead of structure factor, $S(Q)$. This is because (1) it is difficult to define the interparticle structure factor due to the hierarchy of structure, (2) the silica particles are not isotropic and its rotation under elongation itself may induce anisotropic particle structure, and (3) polydispersity in particle shape and size prevent us from justifying the simple factorization of scattering intensity into interparticle structure factor and particle structure factor (eq. (2)). The scattering intensity was accordingly expanded in terms of spherical harmonics, and the coefficient, $I_l^0(Q,t_j)$, was calculated at each t_j, namely:

$$I_l^0(Q,t_j) = \tfrac{1}{2}\int_0^\pi I(Q,\theta,t_j)Y_l^0(\theta)\sin\theta d\theta. \quad (6)$$

Then, the averaged coefficient was calculated by

$$I_{l\,\mathrm{avg}}^0(Q) = \tfrac{1}{10}\sum_{j=1}^{10} I_l^0(Q,t_j). \quad (7)$$

To discuss the changes in the spherical harmonics coefficient during cyclic strain, we defined a normalized coefficient, $A_l^0(Q,t_j)$, by

$$A_l^0(Q,t_j) = \frac{I_l^0(Q,t_j)}{I_{l\,\mathrm{avg}}^0(Q)}. \quad (8)$$

Results and discussion

SAXS intensity profiles

Figure 2 (upper) shows $I(Q)$ of S1, S2, and S3 before stretching. The scattering intensity profiles have two characteristics regardless of the number of silica particles: One is the presence of the shoulder at approximately

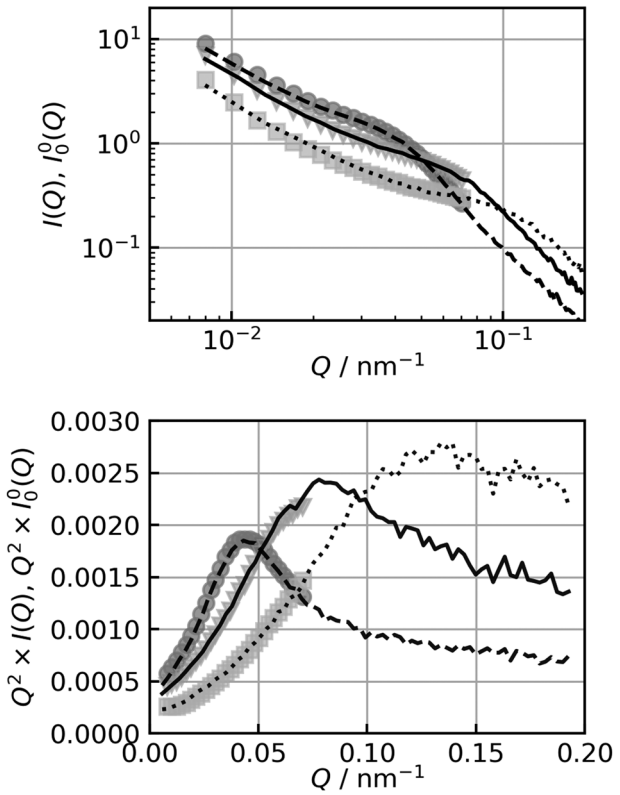

Fig. 2 (Upper) SAXS intensity profiles, $I(Q)$, and (lower) their Kratky plot, $Q^2 \times I(Q)$, for the samples using Si266 as a silane-coupling agent: (dashed line) S1, (solid line) S2, and (dotted line) S3. $I_0^0(Q)$ and $Q^2 I_0^0(Q)$ are also shown in the upper and lower figures, respectively: (circles) S1, (triangles) S2, and (squares) S3. For clarity, the values of $I_0^0(Q)$ are multiplied by 1.1

$0.04 < Q/\mathrm{nm}^{-1} < 0.1$, which corresponds to the correlation between silica aggregates as discussed in previous work using the same silica particles in styrene–butadiene rubber [29], and the other is an upturn toward a low-Q ($Q/\mathrm{nm}^{-1} < 0.02$). Most of the previous studies of filled rubber using SAXS suggest the existence of a higher order structure. Meanwhile, the finite coherent length of X-rays may contribute to this upturn [30]. We thus do not discuss this low-Q behavior in this paper. All of the other samples showed similar intensity profiles.

The position of the shoulders becomes clear by using the Kratky plot [10], Q vs $Q^2 \times I(Q)$, as shown in Fig. 2 (lower). The peak position in the Kratky plot corresponds to the location of the shoulder. The Kratky plot can also be used for a two-dimensional scattering image as shown in Fig. 1d. As the volume fraction of silica increases, the distance between silica aggregates will be shortened, which results in a shift of peak position toward high-Q in the Kratky plot. The averaged distance between silica aggregates, d_c, can be roughly estimated by the inverse of peak position, $2\pi/Q_c$, where Q_c is the peak position in the Kratky plot. The calculated values of d_c for samples before stretching are also summarized in Table 1.

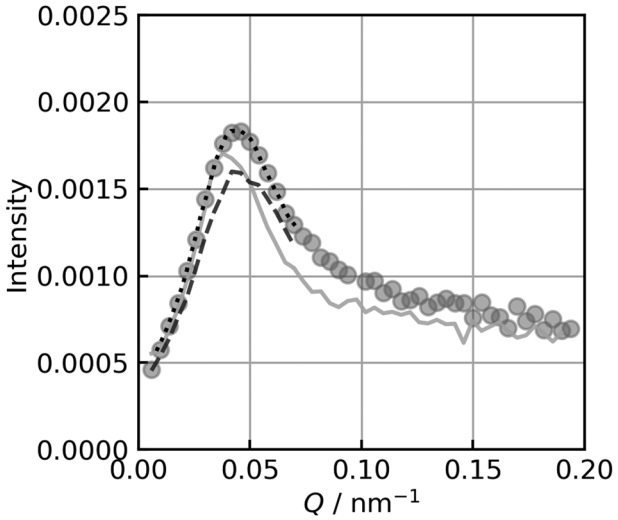

Fig. 3 Kratky plot of S1 at 25 °C: (circles) $Q^2 \times I(Q)$ of undeformed sample, (solid line) $Q_z^2 \times I(Q_z)$ of stretched sample, (dashed line) $Q_x^2 \times I(Q_x)$ of stretched sample, (dotted line) $Q^2 \times I_0^0(Q)$ of stretched sample. The stretched sample shows the result of those with $f = 10$ Hz and measured during $t = 45$–55 ms

Stretching of the sample $\left(\frac{\Delta L}{L_0} = 0.2\right)$ resulted in subtle changes in scattering intensity profiles as shown in Fig. 1c,d for Si266 (S1) at 25 °C and $0.45\,T < t < 0.55\,\mathrm{T}$ ($f = 10$ Hz: $T = 0.1$ s). Anisotropy due to the stretching is hardly observed, and the Kratky image (Fig. 1d) shows a somewhat elliptical ring originating from the correlation between neighboring particles. Following a conventional analysis scheme that focuses on the scattering intensities along the parallel and perpendicular directions, the Kratky plot of one-dimensional scattering intensity profiles, $I(Q_x = 0, Q_z)$ and $I(Q_x, Q_z = 0)$, of a stretched sample is calculated (Fig. 3). The result of $Q^2 \times I(Q_x = 0, Q_z)$ shows a slight shift in the peak position toward a lower-Q, whereas that of $Q^2 \times I(Q_x, Q_z = 0)$ shows the appearance of a shoulder at around $Q = 5.5 \times 10^{-2}\,\mathrm{nm}^{-1}$. These behaviors were independent of the sample type and measurement conditions. Traditionally, the peak shift in the Kratky plot has been used to discuss the structural changes of filler aggregate upon stretching. It is, however, just a projected structure in three-dimensional reciprocal space and ignores scattering information along with other directions. A quantitative discussion is also difficult: for example, we cannot determine whether the whole structure deforms in a way suggested by the projected Kratky plot. Thus, we need to proceed to the analysis using spherical harmonics expansion.

Spherical harmonics expansion analyses of stretched rubber SAXS

Using the real spherical harmonic expansion approach, we can make a more quantitative discussion about the

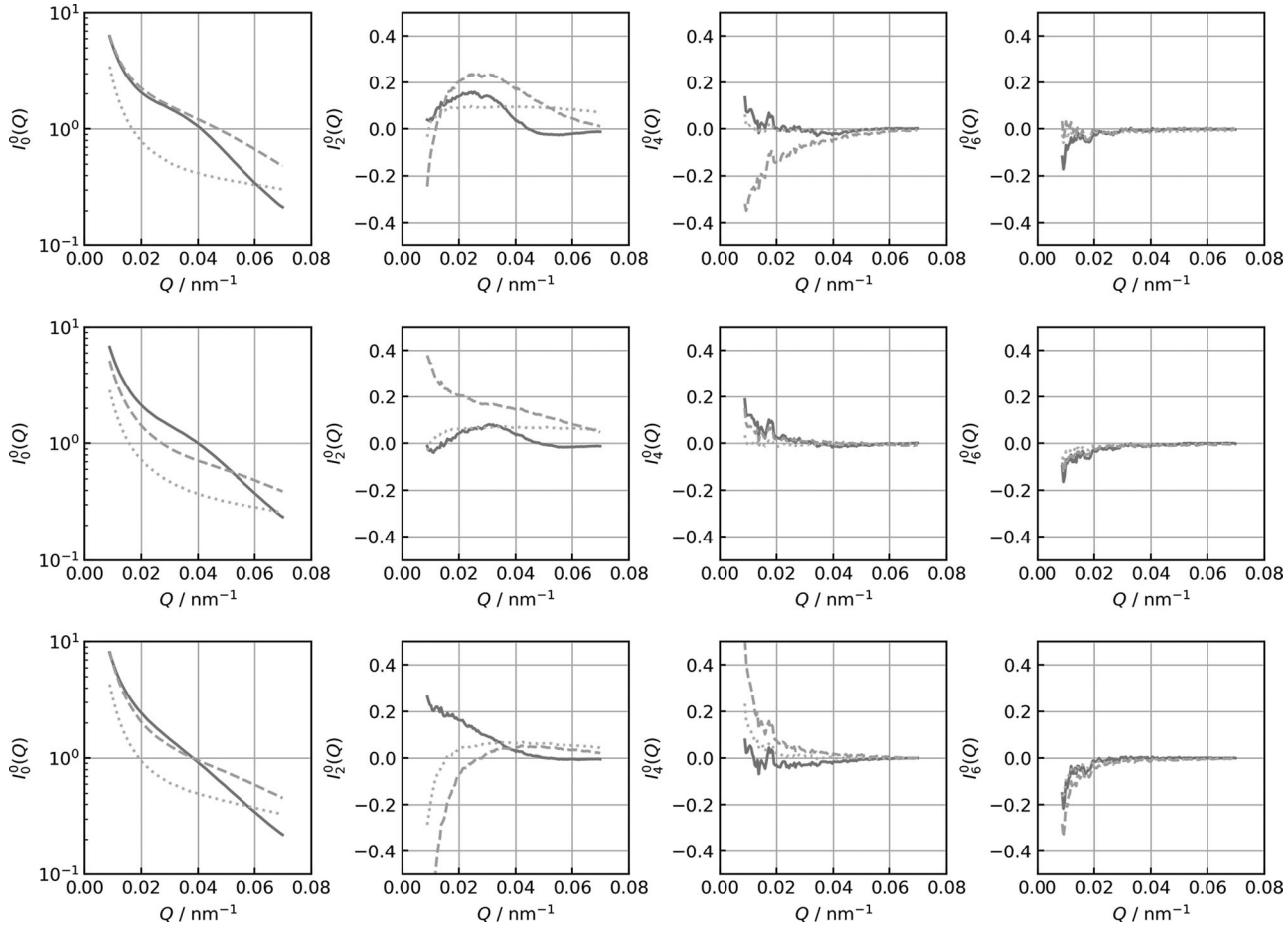

Fig. 4 Spherical harmonics expansion coefficient (upper) without coupling agent (W1, W2, and W3), (middle) with Si266 (S1, S2, S3), and (lower) with NXT (N1, N2, N3) for $f = 1$ Hz and $T = 25$ °C. From left to right: $I_0^0(Q)$, $I_0^2(Q)$, $I_0^4(Q)$, and $I_0^6(Q)$. (Solid line): W1, S1, and N1, (dashed line) W2, S2, and N2, and (dotted line) W3, S3, and N3

anisotropic structural changes. First, we discuss the averaged structural changes of samples under stretching to $\frac{\Delta L}{L_0} = 0.2$ and ignore the structural changes with cyclic stretching. Spherical expansion coefficients, $I_0^0(Q)$, $I_2^0(Q)$, $I_4^0(Q)$, and $I_6^0(Q)$, of stretched samples at 25 °C and 1 Hz are shown in Fig. 4. Here, the profiles were averaged over a whole period. The shape of the expansion coefficient was more or less independent of the type and presence of silane-coupling agent for $I_0^0(Q)$ and $I_6^0(Q)$, and the shape of $I_2^0(Q)$ highly depends on the silane-coupling agent. The shape of $I_4^0(Q)$ seems to have dependence on the sample only at low Q. The positive sign of $I_4^0(Q)$ means that the scattering intensity is high in the direction along Q_x and/or Q_z directions, whereas the negative sign indicates the presence of a clover-like four-point pattern that shows high scattering intensity along a diagonal direction and is often observed for SAXS of stretched samples. It is expected that this term will be more prominent when $\frac{\Delta L}{L_0}$ is greater than the current study. The dependence of $I_4^0(Q)$ on the sample will be discussed in detail in a future study. In the following, we discuss $I_0^0(Q)$ and $I_2^0(Q)$ of stretched samples in detail. Because the Q-range along the Q_x was limited due to the detector size as shown in Fig. 1c, the maximum Q for the spherical harmonic expansion is unfortunately limited to around 0.07 nm^{-1}. Furthermore, the quality of expansion at low Q ($Q < \sim 0.02$ nm^{-1}) is low particularly for the anisotropic coefficients, $I_2^0(Q)$, $I_4^0(Q)$, and $I_6^0(Q)$ because of the small number of pixels used for calculating the expansion coefficients at low Q.

The isotropic coefficient, $I_0^0(Q)$, shows almost identical profiles as those of samples without stretching (Figs. 2 and 3). Even though the Q-range is limited, the agreement between the profile of the isotropic part of the stretched sample and that of the unstretched sample is remarkable. Indeed, the ratio between $I_0^0(Q)$ of the stretched sample and $I(Q)$ of the unstretched sample was almost constant at $0.02\,\text{nm}^{-1} < Q < 0.07\,\text{nm}^{-1}$ with $I_0^0(Q)/I(Q)$ of 0.85–0.95. The Q^2-weighted isotropic part, $Q^2 I_0^0(Q)$, should have shown some broadening compared to the undeformed sample if the sample is homogeneously deformed [31]. The fact that no broadening is observed and that the ratio between the isotropic part and scattering intensity shows a high value

(~0.9) indicates that the structural changes inside samples are not homogeneous at all: most of the filler aggregate structure does not deform at this stretching ratio, and a small fraction of sample shows anisotropic deformation as discussed in the following.

The profiles of $I_2^0(Q)$ show anisotropic deformation of the silica aggregate configuration. When the volume fraction of silica is small (W1, S1, and N1), $I_2^0(Q)$ reaches to zero at around 0.045 nm^{-1} regardless of sample type, temperature, and stretching frequency. This position agrees with the peak position in the Kratky plot of the *unstretched* sample, Q_c, and accordingly corresponds to the averaged interaggregate distance of *unstretched* samples. We can, therefore, confirm that the anisotropic structural changes originate from structural anisotropy of interaggregate structures and not from a change in the intra-aggregate structure nor that in the aggregate structure itself. The negative sign at $Q > Q_c$, particularly for W1, may indicate that the anisotropic silica particles align its long-axis to the stretching direction, which needs to be examined in a future study. The profiles of $I_2^0(Q)$ depend on the sample types, indicating that the different types of silane-coupling agents result in structural anisotropy induced by the uniaxial stretching. Conversion of every spherical harmonics coefficient into real-space pair-distribution functions, $g_l^m(r)$, will help discuss the details as is demonstrated in other studies [18, 19, 22], which will be conducted with more extensive measurements at a high-Q in the future.

Response of filler aggregate structure to cyclic strain

Figure 5 shows time-dependent anisotropic factor $A_l^0(Q,t_j)$ (eq. (8)) of S1 for $l = 0,2$ averaged over 2.9×10^{-2} $nm^{-1} < Q < 6.5 \times 10^{-2}$ nm^{-1} with $f = 0.1$ Hz. The normalized isotropic factor, $A_0^0(Q,t_j)$, was independent of time, indicating that the isotropic component of sample structure did not change under cyclic strain as is expected by the result that the prestretch hardly changed the isotropic component. All of the other samples showed similar behavior. Meanwhile, $A_2^0(Q,t_j)$ showed sinusoidal changes under cyclic strain. Again, most of the other samples showed a similar sinusoidal response except those at Q~Q_c, where the anisotropic factor $A_2^0(Q,t_j)$ cannot be defined because $I_2^0(Q_c)$ is close to zero.

To extract the information about the microscopic response to macroscopic sinusoidal strain, we fit $A_2^0(Q,t_j)$ with the following function:

$$A_2^0(Q,t_j) = -A_2^0(Q)\sin\left(2\pi f t_j - \delta(Q)\right). \quad (9)$$

Here, the amplitude, $A_2^0(Q)$, represents the amplitude of changes in anisotropic structure upon cyclic stretching and

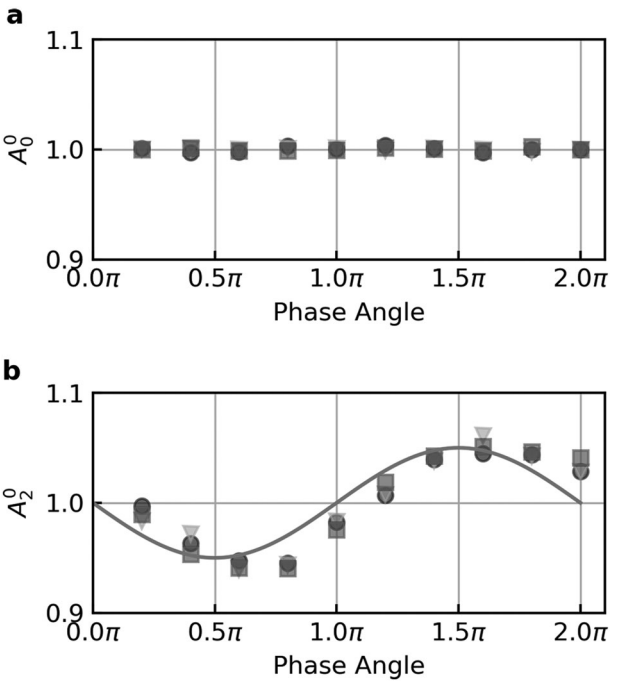

Fig. 5 Normalized coefficient (**a**) $A_0^0(Q,t_j)$ and (**b**) $A_2^0(Q,t_j)$ of S1 with $f = 0.1$ Hz. The values were averaged for 2.9×10^{-2} $nm^{-1} < Q < 6.5 \times 10^{-2}$ nm^{-1}. The temperature was (circle) 0 °C, (triangles) 25 °C, and (squares) 50 °C. The line in (**b**) shows a sinusoidal curve without phase delay

the phase, $\delta(Q)$, corresponds to the microscopic phase delay of anisotropic structure in responding to the cyclic macroscopic uniaxial stretching. We ignored higher-order terms in a sinusoidal function because the number of temporal data points is not large enough to examine the existence of higher-order terms. The results of fitting are shown in Figs. 6 and 7. The results for different temperatures are arranged into a single dataset because of the absence of temperature dependence as shown in the figures. The amplitude, $A_2^0(Q)$, shows little dependence on the sample temperature, frequency, and Q except for the S1 sample. Meanwhile, the phase, $\delta(Q)$, shows a clear frequency dependence. Regardless of the sample type, the samples under cyclic stretching with $f = 0.1$ Hz show a finite phase delay with around $\tan\delta = 0.7$, whereas those with $f = 1$ and 10 Hz are sparsely distributed around zero except for N1. To the best of our knowledge, this is the first observation of delayed response of anisotropic structure upon macroscopic cyclic strain. Structural studies of a deformed sample have been mostly limited to a study of steady-state structure. The results demonstrate the importance of in situ measurements using highly brilliant X-rays from synchrotron sources in studying the structural changes under deformation. Further studies will provide a model for explaining the frequency dependence and the dependence on the silane-coupling agent.

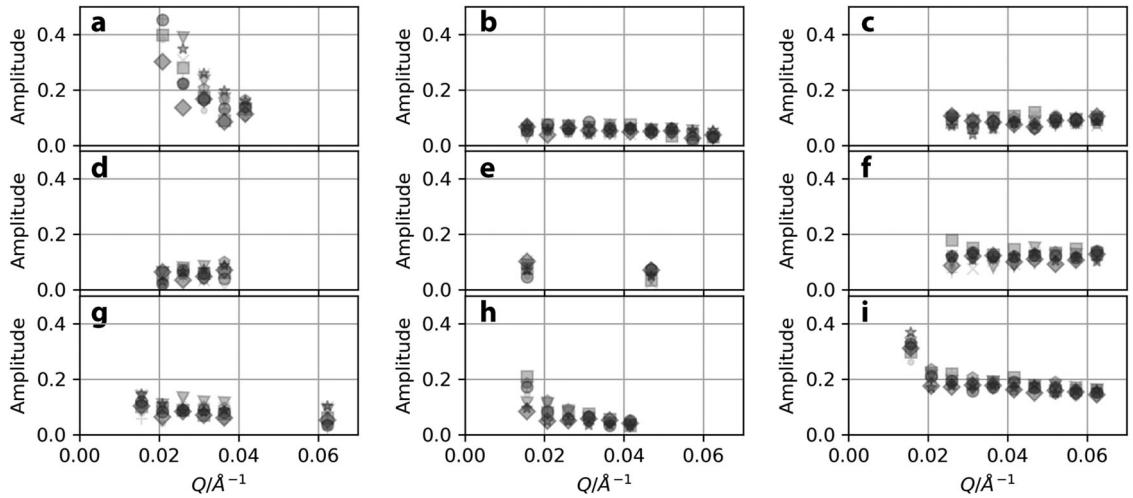

Fig. 6 Q-dependent amplitude, $A_2^0(Q)$, of microscopic structural response: **a** S1, **b** S2, **c** S3, **d** N1, **e** N2, **f** N3, **g** W1, **h** W2, and **i** W3. Each symbol represents the dependence on f and temperature: (squares) 0.1 Hz and 0 °C, (pentagon) 0.1 Hz and 25 °C, (triangles) 0.1 Hz and 50 °C, (dots) 1 Hz and 0 °C, (+) 1 Hz and 25 °C, (×) 1 Hz and 50 °C, (diamonds) 10 Hz and 0 °C, (circles) 10 Hz and 25 °C, and (stars) 10 Hz and 50 °C

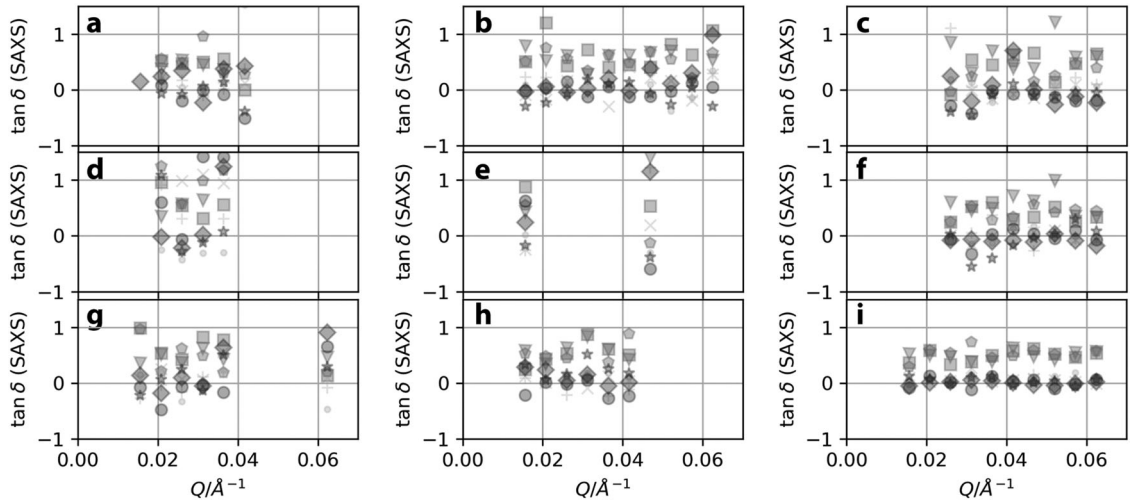

Fig. 7 Tangent of phase delay in $A_2^0(Q,t_j)$: $\tan\delta(Q)$. **a** S1, **b** S2, **c** S3, **d** N1, **e** N2, **f** N3, **g** W1, **h** W2, and **i** W3. See Fig. 6 for the symbols

XPCS of stretched samples

A typical two-time correlation function, $G(Q,t_1,t_2)=\frac{I(Q,t_1)I(Q,t_1)_\phi}{I(Q,t_1)_\phi I(Q,t_2)_\phi}$, of stretched rubber (W2) at $0.024\,\mathrm{nm}^{-1}<Q<0.026\,\mathrm{nm}^{-1}$ is shown in Fig. 8, where the subscript ϕ indicates that the averaging is performed on the pixels corresponding to a range of pixels, $Q\pm\Delta Q$ [32, 33]. The two-time correlation function represents the correlation of scattering intensity at $t=t_1$ and $t=t_2$ and a good measure of dynamics for a temporally evolving system. The color represents the value at a point (t_1, t_2), and the diagonals from the lower left to the upper right of the panels correspond to $\Delta t=0$, where $\Delta t=t_1-t_2$ is the time difference. A calculation was made for both parallel (Q_z) and perpendicular (Q_x) to the stretching, and the intensity was averaged over an azimuthal angle of ±10°. The results show intermittent relaxation as is clear from the rectangular pattern in the two-time correlation functions, which has been observed for metallic glass [34]. These intermittent changes are totally different from the more or less smooth slowing down/speeding up that is observed for stationary samples or samples showing nonequilibrium dynamics [35, 36]. Such an intermittent change was not observed for the samples without stretching. Note that the timing of intermittent changes in two time correlation functions in directions parallel and perpendicular to the stretching is independent of each other. This suggests that this intermittent relaxation is not from macroscopic changes such as an unexpected slip at the chuck of the stretching instrument nor the fluctuations

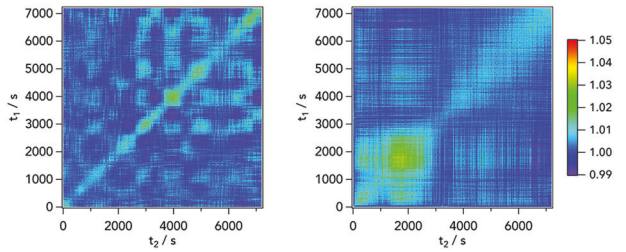

Fig. 8 Two-time correlation images of stretched rubber (W2) at $0.024 < Q/\mathrm{nm}^{-1} < 0.026$: (left) Q_x and (right) Q_z direction

of beam position on the sample but rather from the microscopic changes in the positional correlation between silica aggregates. The intermittent changes occur more frequent in the Q_x direction in Fig. 8, but other samples show the opposite trend.

The presence of inhomogeneous intermittent dynamics is justified by the results of SAXS. A significant amount of isotropic components observed in the SAXS measurement indicates that the samples were mostly undeformed even under uniaxial stretching. Such an inhomogeneous structural deformation will reasonably exhibit temporally unsteady relaxation.

The results showed the absence of flow-like motions that were observed for the stretched rubber as a sinusoidal oscillation in a previous study [25]. All the measured samples show similar anisotropic intermittent dynamics with the averaged relaxation time sparsely distributed around 1×10^3 s. Because of this intermittence, the averaged values will not have a significant meaning. Furthermore, the existence of a large amount of undeformed isotropic structure seems to preclude the observation of anisotropic dynamics. In this regard, the measurement of speckle echoes [37] rather than a simple correlation of speckles will be useful.

Correlation between macroscopic viscoelasticity and microscopic structural response

Our goal in this study is to understand the macroscopic viscoelasticity directly based on the microscopic structure and dynamics of filled rubber. To explore the correlation, we plotted the values of microscopic $\tan\delta$ in anisotropic structural change that was estimated by the temporal change (Fig. 7) and viscoelastic $\tan\delta$ that was simultaneously measured during the SAXS experiments in Fig. 9. Indeed, there is no correlation between $\tan\delta$ of anisotropic structural change and viscoelastic $\tan\delta$. The lack of correlation in this study may be attributed to several reasons: (1) the contribution of rubber polymer networks is ignored because the current SAXS analysis cannot observe the structural change of rubber polymer networks, and (2) only a tiny fraction of

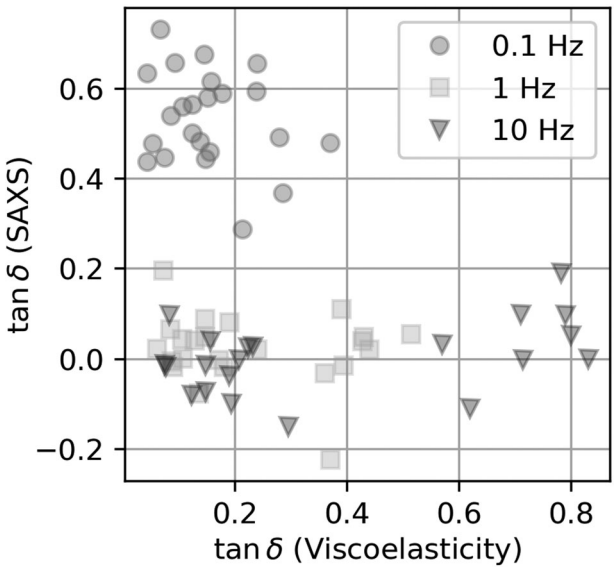

Fig. 9 Correlation between $\tan\delta$ measured by SAXS and that measured by viscoelastic measurement. The inset indicates the frequency of the cyclic strain

samples contributes to the anisotropic part, $S_2^0(Q)$, and the majority of the sample does not show the microscopic change in the filler structures as suggested by $S_0^0(Q)$ of stretched samples. Concerning the first point, it is rubber polymer networks that show a characteristic rubber elasticity, and the nanoparticles play a significant role in changing the viscoelastic properties. Thus, it is natural that the structural response of rubber polymer networks needs to be included when discussing the relationship between microscopic structural response and macroscopic viscoelasticity. Neutron scattering studies as well as wide-angle X-ray scattering will complement the current SAXS studies and will provide a complete picture of the structural changes of filled rubber under stretching. The second point is more crucial because this shows the significant presence of structural and elastic heterogeneities and the observed structural changes of nanoparticles cannot be directly related to the macroscopic viscoelasticity. This has, in fact, been recognized by many groups through the observation of higher-order structure and butterfly pattern in SAXS and SANS of stretched rubber and gel but is implicitly ignored in regard to discussing the correlation between microscopic structures and macroscopic properties such as viscoelasticity. This inhomogeneity makes it complicated to relate microscopic structures and macroscopic viscoelastic properties. In that sense, the analyses using spherical harmonics expansion can provide not only a thorough tool for the anisotropic structural analysis but also relevant information regarding the structural inhomogeneity through the quantitative analysis of the isotropic component.

Conclusions

Structural changes of silica aggregates under cyclic strain were measured with time-resolved SAXS. Scattering data were decomposed into the anisotropic and isotropic components by using a spherical harmonics expansion approach. Even though stretched samples show anisotropic scattering profiles as a whole, the result of decomposition showed that the scattering intensity was dominated by an isotropic component, which agrees with the scattering intensity profiles of the undeformed sample. This indicates an inhomogeneous structural response upon uniaxial elongation, at least for $\frac{\Delta L}{L_0} = 0.2$. Delay in structural response was observed for the cyclic strain with $f = 0.1$ Hz, but no correlation between this delay and the macroscopic loss tangent was found. This study demonstrates that analyses using spherical harmonics are quite useful for discussing anisotropic structural changes in the filler aggregate/agglomerate. Further scattering studies over a wide Q-range utilizing this approach will clarify the detailed anisotropic response to the external field.

Acknowledgements We thank Hiroyasu Masunaga (JASRI/SPring-8) for his support at BL03XU. The SAXS and XPCS measurements were supported by Chikara Sasaki and Daiki Kikutake (University of Tokyo) and were conducted under the approval of SPring-8 Proposal Review Committee (Proposal No. 2014A1287, 2014A7209, 2014B1490, 2014B7259, 2015A1625, 2015A7209, 2015B1425, 2015B7259, 2016A1368, 2016A7209, 2016B1512, 2016B7209). Preliminary measurements of XPCS were conducted at BL40XU, SPring-8 (Proposal No. 2014B1069). This study was partially supported by "Photon and Quantum Basic Research Coordinated Development Program" from the Ministry of Education, Culture, Sports, Science and Technology, Japan. Y.S. is thankful for the discussion with Wei-Ren Chen (ORNL). The authors declare no competing financial interests.

Compliance with ethical standards

Conflict of interest The authors declare that they have no conflict of interest.

References

1. Koga T, Hashimoto T, Takenaka M, Aizawa K, Amino N, Nakamura M, et al. New insight into hierarchical structures of carbon black dispersed in polymer matrices: a combined small-angle scattering study. Macromolecules. 2008;41:453–64.
2. Koga T, Takenaka M, Aizawa K, Nakamura M, Hashimoto T. Structure factors of dispersible units of carbon black filler in rubbers. Langmuir. 2005;21:11409–13.
3. Hyeon-Lee J, Beaucage G, Pratsinis S, Vemury S. Fractal analysis of flame-synthesized nanostructured silica and titania powders using small-angle X-ray scattering. Langmuir. 1998;14:5751–6.
4. Schaefer D, Rieker T, Agamalian M, Lin J, Fischer D, Sukumaran S, et al. Multilevel structure of reinforcing silica and carbon. J Appl Cryst. 2000;33:587–91.
5. Kammler HK, Beaucage G, Mueller R, Pratsinis SE. Structure of flame-made silica nanoparticles by ultra-small-angle X-ray scattering. Langmuir. 2004;20:1915–21.
6. Baeza GP, Genix A-C, Degrandcourt C, Petitjean L, Gummel J, Oberdisse J. Multiscale filler structure in simplified industrial nanocomposite silica/SBR systems studied by SAXS and TEM. Macromolecules. 2012;46:317–29.
7. Kishimoto H, Shinohara Y, Amemiya Y, Inoue K, Suzuki Y, Takeuchi A, et al. Structural analysis of filler in rubber composite under stretch with time-resolved two-dimensional ultra-small-angle X-ray scattering. Rubber Chem Tech. 2008;81:541–51.
8. Genix A-C, Oberdisse J. Structure and dynamics of polymer nanocomposites studied by X-ray and neutron scattering techniques. Curr Opin Colloid Interface. 2015;20:293–303.
9. Ehrburger-Dolle F, Bley F, Geissler E, Livet F, Morfin I, Rochas C. Filler networks in elastomers. Macromol Symp. 2003;200:157–67.
10. Ehrburger-Dolle F, Hindermann-Bischoff M, Livet F, Bley F, Rochas C, Geissler E. Anisotropic ultra-small-angle X-ray scattering in carbon black filled polymers. Langmuir. 2001;17:329–34.
11. Mendes J Jr., Lindner P, Buzier M, Boué F, Bastide J. Experimental evidence for inhomogeneous swelling and deformation in statistical gels. Phys Rev Lett. 1991;66:1595–8.
12. Bastide J, Leibler L, Prost J. Scattering by deformed swollen gels—butterfly isointensity patterns. Macromolecules. 1990;23:1821–5.
13. Koizumi S, Monkenbusch M, Richter D, Schwahn D, Farago B. Concentration fluctuations in polymer gel investigated by neutron scattering: Static inhomogeneity in swollen gel. J Chem Phys. 2004;121:12721–31.
14. Oberdisse J. Aggregation of colloidal nanoparticles in polymer matrices. Soft Matter. 2006;2:29–36.
15. Pyckhout-Hintzen W, Urban V, Belina G, Straube E, Kluppel M, Heinrich G. Microscopic deformation of filler particles in rubber under uniaxial deformation. Macromol Symp. 2003;200:121–8.
16. Nishi K, Shibayama M. 2D pair distribution function analysis of anisotropic small-angle scattering patterns from elongated nanocomposite hydrogels. Soft Matter. 2017;13:3076–83.
17. Kishimoto H, Shinohara Y, Suzuki Y, Takeuchi A, Yagi N, Amemiya Y. Pinhole-type two-dimensional ultra-small-angle X-ray scattering on the micrometer scale. J Synchrotron Rad. 2014;21:1–4.
18. Wang Z, Lam CN, Chen W-R, Wang W, Liu J, Liu Y, et al. Fingerprinting molecular relaxation in deformed polymers. Phys Rev X. 2017;7:179–17.
19. Huang G-R, Bin W, Wang Y, Chen W-R. Characterization of microscopic deformation through two-point spatial correlation functions. Phys Rev E. 2018;97:012605.
20. Suzuki Y, Haimovich J, Egami T. Bond-orientational anisotropy in metallic glasses observed by x-ray diffraction. Phys Rev B. 1987;35:2162–8.
21. Hess S. Shear-flow-induced distortion of the pair-correlation function. Phys Rev A. 1980;22:2844–8.
22. Dmowski W, Iwashita T, Chuang CP, Almer J, Egami T. Elastic heterogeneity in metallic glasses. Phys Rev Lett. 2010;105:205502.
23. Wagner NJ, Ackerson BJ. Analysis of nonequilibrium structures of shearing colloidal suspensions. J Chem Phys. 1992;97:1473–83.
24. Livet F, Bley F, Ehrburger-Dolle F, Morfin I, Geissler E, Sutton M. X-ray intensity fluctuation spectroscopy by heterodyne detection. J Synchrotron Rad. 2006;13:453–8.
25. Ehrburger-Dolle F, Morfin I, Bley F, Livet F, Heinrich G, Richter S, et al. XPCS investigation of the dynamics of filler particles in stretched filled elastomers. Macromolecules. 2012;45:8691–701.

26. Kraft P, Bergamaschi A, Broennimann C, Dinapoli R, Eikenberry EF, Henrich B, et al. Performance of single-photon-counting PILATUS detector modules. J Synchrotron Rad. 2009;16:368–75.
27. Masunaga H, Ogawa H, Takano T, Sasaki S, Goto S, Tanaka T, et al. Multipurpose soft-material SAXS/WAXS/GISAXS beamline at SPring-8. Polym J. 2011;43:471–7.
28. Shinohara Y, Imai R, Kishimoto H, Yagi N, Amemiya Y. Indirectly illuminated X-ray area detector for X-ray photon correlation spectroscopy. J Synchrotron Rad. 2010;17:737–42.
29. Shinohara Y, Kishimoto H, Yagi N, Amemiya Y. Microscopic observation of aging of silica particles in unvulcanized rubber. Macromolecules. 2010;43:9480–7.
30. Shinohara Y, Amemiya Y. Effect of finite spatial coherence length on small-angle scattering. J Appl Cryst. 2015;48:1660–4.
31. Wang Z, Iwashita T, Porcar L, Wang Y, Liu Y, Sanchez-Diaz LE, et al. Local elasticity and dynamical heterogeneity in nonlinear rheology of interacting colloidal glasses revealed by neutron scattering and rheometry. arXiv. 2016;1611:03135.
32. Livet F, Abernathy DL, Bley F, Caudron R, Geissler E, Detlefs C, et al. Kinetic evolution of unmixing in an AlLi alloy using X-ray intensity fluctuation spectroscopy. Phys Rev E. 2001;63:036108.
33. Sutton M, Laaziri K, Livet F, Bley F. Using coherence to measure two-time correlation functions. Opt Express. 2003;11:2268–77.
34. Evenson Z, Ruta B, Hechler S, Stolpe M, Pineda E, Gallino I, et al. X-ray photon correlation spectroscopy reveals intermittent aging dynamics in a metallic glass. Phys Rev Lett. 2015;115:175701.
35. Conrad H, Lemkühler F, Fischer B, Westermeier F, Schroer MA, Chushkin Y, et al. Correlated heterogeneous dynamics in glass-forming polymers. Phys Rev E. 2015;91:042309.
36. Madsen A, Leheny RL, Guo H, Sprung M, Czakkel O. Beyond simple exponential correlation functions and equilibrium dynamics in X-ray photon correlation spectroscopy. New J Phys. 2010;12:055001.
37. Rogers MC, Chen K, Andrzejewski L, Narayanan S, Ramakrishnan S, Leheny RL, et al. Echoes in X-ray speckles track nanometer-scale plastic events in colloidal gels under shear. Phys Rev E. 2014;90:062310.